A Passively Adaptive Rotary-to-Linear Continuously Variable Transmission

Joseph T. Belter and Aaron M. Dollar, *Senior Member, IEEE*

***Abstract*—In this paper, we present the synthesis and design of a rotary-to-linear continuously variable transmission with the ability to passively change gear ratio as a function of the output load. The primary mechanism involves variable-pitch rollers whose angle changes as a function of the output load due to the compliance properties of their housing. By changing spring stiffness, the relationship between the linear output load and transmission ratio can be tuned to optimize drive motor operating conditions over the entire range of output loads. After laying out the working concept, we show the performance analysis for such a transmission applied to a 6-W DC motor and present an example design analysis for tuning to maximize power output over the entire range of operating conditions. A prototype system was used to measure key parameters such as rolling resistance and lateral slip coefficients and to evaluate the transmission performance in a target application.**

***Index Terms*—Constant power, continuously variable transmission (CVT), linear actuator, passive adaptive, underactuated.**

I. Introduction

NEARLY all actuation technologies have a narrow peak efficiency or power region. In the design of mechatronic systems, it is common practice to choose a transmission ratio that places the operating point of the motor in this narrow region for a given application. In cases where the actuator must be used in a range of output performance conditions, the transmission would ideally be variable to keep the actuator operating near the peak efficiency or peak power region. However, variable transmissions, which generally switch between a small number of discrete transmission ratios, typically require significant additional mechanical complexity, weight, and size, as well as additional sensors and actuators to reconfigure the transmission. Extending the concept, continuously variable transmissions (CVT) have similar shortcomings.

We present a concept (see Fig. 1) that has a number of significant advantages over traditional variable transmissions. First, the ratio varies passively and continuously with the output load (see Fig. 1(b)), eliminating the need for additional sensing, actuation, and control to obtain the proper transmission ratio. Second, the concept is simple enough to be compactly implemented in a small and lightweight package. Third, it is one of few rotary-to-linear transmission concepts.

Manuscript received August 12, 2013; revised April 1, 2014; accepted June 13, 2014. Date of publication September 9, 2014; date of current version September 30, 2014. This paper was recommended for publication by Editor B. J. Nelson upon evaluation of this reviewers' comments. This work was supported in part by the Gustavus and Louis Pfeiffer Foundation.

The authors are with the Department of Mechanical Engineering and Material Science, Yale University, New Haven, CT 06510 USA (e-mail: joseph.belter@yale.edu; aaron.dollar@yale.edu).

Color versions of one or more of the figures in this paper are available online at http://ieeexplore.ieee.org.

Digital Object Identifier 10.1109/TRO.2014.2333096

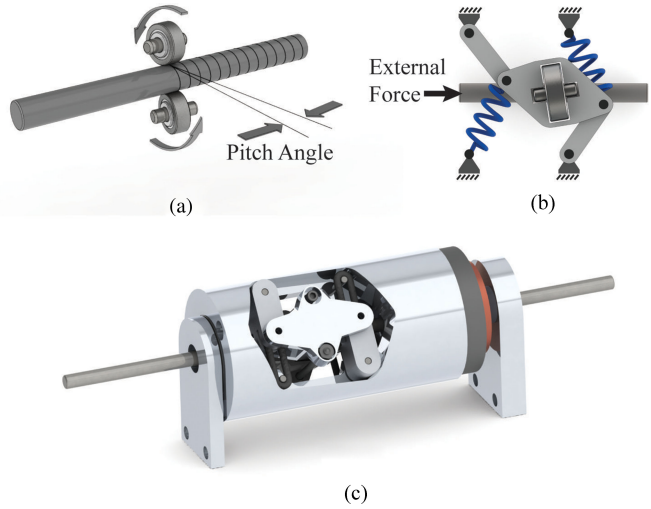

Fig. 1. Novel linear passive CVT makes use of a compliant Watt straight-line mechanism (b) to alter the pitch angle of a set of rollers (a) around a center shaft. The transmission is can be packaged within the diameter of a small out-runner brushless motor (c).

There are a number of applications, such as in mobile robotics, where the actuator power-to-weight ratio is an important performance factor. In legged locomotion, for example, there is typically a repetitive cycle of stance and swing phases—the former generally requires high force/torque and low speed movements (while the foot is on the ground), while the latter involves relatively little force but at large motions/speeds (while the foot is moving through the air) [1]. By increasing the delivered power of the actuator throughout the entire operating range using a simple and lightweight CVT, the overall power-to-weight ratio can be improved. Ideally, a transmission for this application would have a relatively small step-down ratio for the swing phase (to keep speeds high under low loads) and would switch to a larger ratio for the stance phase. Similarly, for grasping and manipulation, it is generally desired to have high speeds during finger closure (under low loads) and high forces/torques for grasp strength (with low/no motion). There is extensive work on the design of such switching transmissions for grasping [2].

There has been a large amount of related work in actively controlled CVTs, which are commonly used commercially in automobiles. Most of these operate by varying the radius at which a belt or roller draws power from the actuating shaft [3]. Within the field of robotics, researchers have implemented variable-radius rollers in a fashion similar to an automotive CVT [4]. Alternative CVT designs have been proposed in robotics, such as variable-moment arm actuators [5] and noncircular gear pairs [6] (which showed a 24% increase in robot jumping height,

as compared with the optimal fixed-ratio system). One example of a variable pitch roller transmission used in a robot system is a type of Cobot architechure [7] that consists of a rotation drum feeding power to a roller placed axially along the drum. By controlling the angle of the roller relative to the axis of the drum, the roller and roller housing translate at a rate proportional to the tangent of the roller angle. All of these and similar systems change ratio actively, through the use of an additional actuator, or vary the ratio as a direct function of position.

In terms of passively variable or load-sensitive transmissions, in which the desired relationship between output load and gear ratio can be used to passively change the transmission ratio, a few related works have been found. For example, stepping through the gear ratios of standard bicycles can be achieved as a function of road speed to keep the pedal speed within a desirable range [8]. One passive rotary CVT mechanism developed is a toroidal rotary CVT [9], which uses the output torque to alter the contact radius of a rolling contact element to maintain a constant level of transmitted power. Other passively variable CVT transmissions use a centrifugal-based belt drive that changes the belt radius based on the angular velocity of the pulley [10].

Passive rotary-to-linear CVTs can also be created through five-bar linkage-based designs [11] if only a limited amount of output travel is necessary. One attempt at producing a passive rotary-to-linear CVT was found on a project called the X-Screw [12]. This actuator is a cycloidal drive (similar to a one-lobe harmonic drive), which operates by rapidly oscillating an oversized nut around a lead screw. The magnitude of the oscillation is determined by the force on the nut, producing an effect on the input rotation to output translation ratio. The primary drawback of this design was its limited efficiency because the power was transmitted from the oscillating nut to the output shaft through a combination of rolling and sliding. One CVT for tendon driven robot hands uses a variable radius drum whose radius changes as a function of the drive torque on the drum [13]. Additional tendon driven-based CVTs have been developed, including [14], which relies on an elastic series element to determine the radius of the drive tendon about a pivot joint.

The most closely related passive transmission to the concept presented in this study was developed for pipe inspection [15]. Here, an angled roller is used to propel the robot forward through the center of a large pipe. The angle of the roller and, therefore, the drive transmission ratio are passively altered based on the load required to move forward though the pipe. One major limitation is that this mechanism only achieves the desired passive ratio change for one direction of motion through the pipe.

The concept described in this paper implements a set of rollers that rotate around a shaft at a certain pitch angle (see Fig. 1(a)), resulting in a system that is functionally similar to Acme, lead, or ball screw systems, where the roller pitch is equivalent to the thread pitch. Two commercially available products use angled rollers on a smooth shaft as a rotary to linear transmission element [16], [17], the first of which has an adjustment lever that can be used to manually choose the effective screw pitch of the mechanism. These transmissions have very low backlash compared with screw drives, and the adjustability of the screw pitch has made them useful in applications where manual pitch adjustment is needed, such as wire and cable winding machines. As in other friction drives, slip can limit the maximum axial output force. However, this limit can be engineered to be fairly high; the two providers referenced, here rate their friction-based transmissions at up to 900 N [17] and 2 kN [16] of axial force.

Since the rollers in the proposed transmission rely on a compliant element to change gear ratio, the system exhibits behavior similar to a series elastic actuator with variable gear ratio. Series elastic actuators [18] rely on a spring element between the stiff input and the desired output to improve force control stability and shock tolerance. Variable stiffness actuator systems have also been developed to better respond to external disturbances [19].

In this paper, we present the analysis and synthesis of a passively variable rotary to linear CVT with the ability to tune the gear ratio as a function of the output force. We first present the transmission concept and discuss the influence of key parameters to system performance (see Section II). We then carefully study the ideal and nonideal behavior of angular rolling transmission elements (see Section III). By combining this analysis with a kinematic study of the Watt four-bar mechanism (see Section IV), we show how to optimize the transmission for a given actuator operating region (see Section V). We finish by presenting the evaluation of a prototype system (see Section VI) designed to keep the DC motor operating in the region of peak electrical efficiency and offer discussion on the practical implementation of the proposed transmission.

II. Transmission Concept

The transmission concept is similar to a ball screw transmission with a variable pitch that enables the transmission ratio to passively adapt to changing load conditions. Fig. 2(d) illustrates the general concept. A smooth shaft is run through the center of a set of rollers. The rollers are supported by an axially constrained "nut," which rotates around the shaft similar to a threaded nut rotating around a threaded rod. The angle of the rollers determines the transmission ratio between rotation of the nut and translation of the center shaft.

Instead of a fixed attachment of the rollers to the rotating nut, as in the traditional angled roller transmissions [16], [17], the rollers of the passive transmission are mounted to the nut at the center point of a Watt straight-line linkage [20], which is shown in Fig. 1(b). The single degree of freedom (DOF) of the four-bar linkage allows for a small amount of lateral translation along the direction of the shaft. As the lateral force transmitted between the roller and the shaft increases, the four-bar linkage system deflects, as shown in Fig. 2(a) and (c). The deflection of the roller through the four-bar linkage in either direction causes a decrease in the pitch angle and, therefore, an increase in the rotary-to-linear transmission ratio. Since the stiffness of the four-bar linkage acts in series with the output force, the desired transmission ratio (roller angle) can be achieved for all output loads by carefully tuning the stiffness of the four-bar linkage. Note that while this example shows the actuator rotating the "nut" with the shaft translation as the output, the system can just as easily accommodate an actuator rotating the shaft with

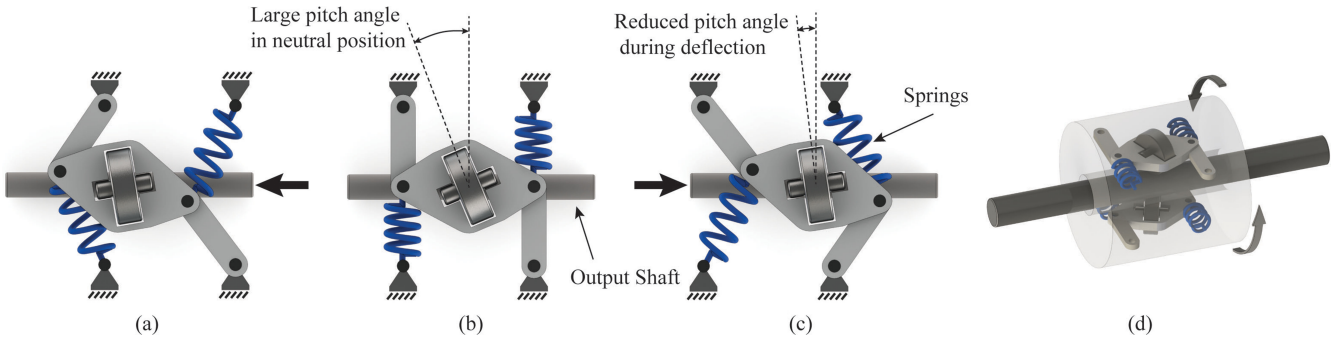

Fig. 2. Critical enabling technology behind the proposed transmission is a simple linkage which changes the pitch angle of the roller as a function of deflection. The load applied in either a pushing or pulling direction [as shown in (a) and (c)] results in a decrease in the pitch angle of the roller and, therefore, an increase in the rotary-to-linear transmission ratio. (b) Image of the linkage in the equilibrium state when no loads are placed on the output shaft. (d) Two linkage systems mounted within a "nut" that rotates around the output shaft. To drive the shaft to the left or right, the nut is rotated either clockwise or counterclockwise.

the nut translation being the output, as in any Acme, lead, or ball screw system. In the following section, we will discuss the details of rolling contact transmission systems.

A. Ideal Angled Roller Behavior

As described in detail in [7] and [21], the use of an angled roller positioned on a shaft acts in a similar manner to a lead screw. Rotational torque is translated into linear force through the angled roller element. In the ideal case, the angle between the perpendicular to the shaft and the plane of the roller, θ, as seen in Fig. 3(a), is the equivalent of the pitch angle of the system. The relationship between the rotational speed of the rollers around the shaft, ω, and the ideal lateral velocity, V_{ideal}, of the shaft (radius r) is

$$V_{\text{Ideal}} = \omega r \tan(\theta). \tag{1}$$

The steady-state force balance is described in (2) and illustrated in Fig. 3(c), where F is the lateral force from the rollers on the output shaft, and τ_{motor} is the torque supplied from the motor to move the rollers around the shaft.

$$F = \frac{\tau_{\text{motor}}}{r \tan(\theta)} \tag{2}$$

Since we are assuming an ideal rolling contact behavior, the rotary input power P_{Input} is equal to the linear output power P_{Output}:

$$P_{\text{Input}} = \tau_{\text{motor}}\omega = F V_{\text{Ideal}} = P_{\text{Output}}. \tag{3}$$

As is the case for any friction-based transmission element, the friction force provides an upper bound to the amount of load transmitted through the system. Therefore, for our roller system, the maximum linear shaft force is described in terms of the number of rollers n_{rollers}, the normal force for each roller F_n, and the friction coefficient between the roller material and the shaft material μ:

$$F \leq F_n n_{\text{rollers}} \mu \cos(\theta). \tag{4}$$

B. Nonideal Angled Roller Behavior

The nonideal characteristics of rolling contact result from the elastic deformation of the two rolling materials at the contact patch. High Hertzian contact stresses are experienced at the contact patch that result in material deformation and microslipping [22], [23]. Although there are many concerns with rolling contacts, including surface wear and other factors, we will focus on the two largest sources of power loss: rolling resistance and lateral slip. These two effects are well characterized for rolling contacts that are within acceptable levels of Hertzian contact stress. In the case of the rollers used for this system, we have assumed similar geometry to two cylinders rolling against each other where the maximum contact pressure σ_{HertzMax} is described as [24]

$$\sigma_{\text{HertzMax}} = \left(\frac{F_n E^*}{\pi w R^*}\right)^{1/2} \tag{5}$$

where $E^* = \left(\frac{1-v_1^2}{E_1} + \frac{1-v_2^2}{E_2}\right)^{-1}$, and $R^* = \left(\frac{1}{r_1} + \frac{1}{r_2}\right)^{-1}$.

Here, v_1 and v_2 are the Poisson ratios of the two roller materials, r_1 and r_2 are the cylinder radii, and w is the width of the contact region. According to [25], manufacturers of modern CVT's with specialized steel rollers require a mean contact stress of less than 2.1 GPa, with a maximum contact stress of 3.15 GPa.

1) Rolling Resistance: Rolling resistance is the dissipated energy during pure rolling of two cylinders contacting each other under normal force F_n. The resulting rolling resistance force is a combination of losses occurring in the roller mounting bearings and at the roller-to-shaft contact patch. The linear relationship can be expressed as a dimensionless coefficient of rolling resistance C_{rr} [26]:

$$F_{\text{rr}} = C_{\text{rr}} F_n. \tag{6}$$

Here, F_{rr} is a force at the contact patch in the direction opposite rolling, as illustrated in Fig. 3(c).

2) Lateral Slip: Lateral slip is the result of lateral elastic deformation of the contact region. It can be shown that lateral slip is a function of the lateral force and the normal force pressure distribution across the contact patch [22]. Equation (7) has been shown to be valid for lateral force values up to approximately 0.7 $F_n n_{\text{rollers}}\ \mu$ and then deviates nonlinearly into gross slip [23]. The coefficient of slip C_{slip} is measured in degrees and

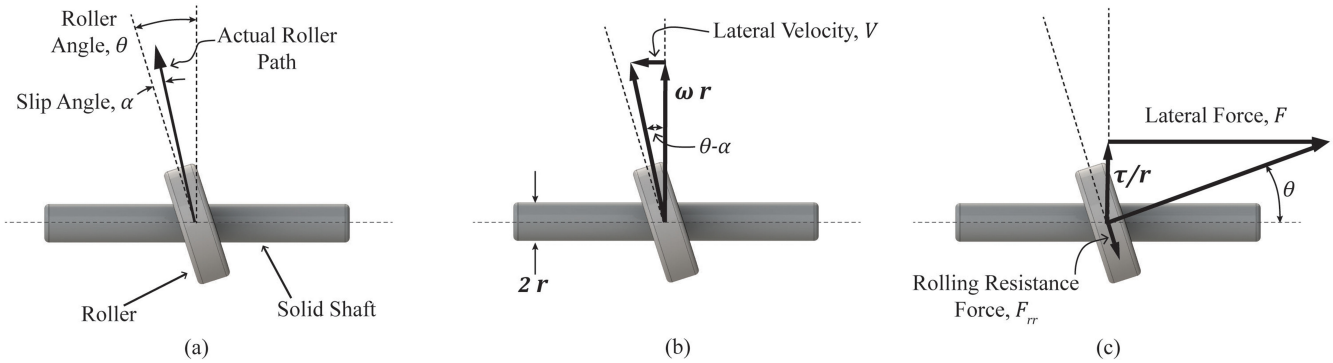

Fig. 3. A smooth roller is pushed against a solid shaft with normal force F_n. The roller angle with respect to the shaft axis determines the transmission ratio between the rotation of the roller around the shaft and the linear output shaft speed. Here, (a) shows the geometric description of the roller and shaft relationship, (b) shows the kinematic relationship, and (c) shows the forces and torques transmited from the roller to the shaft. F is the force from the roller on the output shaft. Lateral velocity V is the roller movement with respect to the shaft.

results in a lateral slip angle α, in degrees. The slip angle is shown in Fig. 3(a).

$$\alpha = C_{\text{slip}} \frac{F}{F_n} \tag{7}$$

The power consumed in the sliding portion of the contact patch P_{slip} can be described by (8). This can also be described as a torque τ_{slip} in (9). The loss is equal to the portion of velocity that is lost as a function of the slip angle. The resulting actual velocity V can be computed using (10) and is illustrated in Fig. 3(b). An important observation from (8) is that the total power lost to lateral slip scales with the portion of roller angle θ lost to slip.

$$P_{\text{Slip}} = FV_{\text{Slip}} = F\left(\omega r \tan\left(\theta\right) - \omega r \tan\left(\theta - \alpha\right)\right) \tag{8}$$

$$\tau_{\text{Slip}} = Fr\left(\tan\left(\theta\right) - \tan\left(\theta - \alpha\right)\right) \tag{9}$$

$$V = \omega r \tan\left(\theta - \alpha\right) \tag{10}$$

After taking all of these nonideal terms into account, we are left with the following relationship(s) to describe the efficiency of the angled roller transmission system (13). Here, P_{input} is the mechanical input power of the drive motor.

$$P_{\text{rr}} = \omega r C_{\text{rr}} F_n n_{\text{rollers}} \tag{11}$$

$$P_{\text{Slip}} = F\omega r\left(\tan(\theta) - \tan\left(\theta - C_{\text{slip}} \frac{F}{F_n n_{\text{rollers}}}\right)\right) \tag{12}$$

$$\varepsilon = (P_{\text{input}} - P_{\text{rr}} - P_{\text{slip}})/P_{\text{input}} \tag{13}$$

III. Design for Maximum Power Application

The goal of a typical CVT transmission is to allow the drive motor to operate in an ideal operating range over a large range of outputs. For typical DC electric motors, the mechanical power and electrical efficiency vary throughout the entire operating range. It is, therefore, desirable to choose a transmission ratio that places the operating point of the motor in or near a region of optimal performance. A variable transmission is necessary if this optimal performance operating region is to be maintained for a wide range of output loads and speeds. In this section, we will determine the optimal transmission ratio and roller angle θ required to keep a DC electric motor operating at the point of maximum mechanical power for all loads F on the output shaft.

The mechanical power of a standard DC electric motor, P_{input}, can be described as a function of the torque output τ, the maximum stall torque τ_{stall}, and the free speed ω_{fs}:

$$P_{\text{input}} = \tau\omega_{fs} - \frac{\tau^2\omega_{fs}}{\tau_{\text{stall}}}. \tag{14}$$

The maximum mechanical power delivered from the motor $P_{\max}$ is achieved when the torque output is equal to half the stall torque as shown in [27] and described by

$$P_{\max} = \frac{1}{2}\tau_{\text{stall}} \cdot \frac{1}{2}\omega_{fs}. \tag{15}$$

A. Desired Roller Angle to Optimize Motor Power

We can use the relationship between motor torque and output force of an ideal angled roller transmission described in (2), to calculate the angle θ necessary to keep the motor torque at $\frac{1}{2}\tau_{\text{stall}}$ (17). The angle is a function of the output force F and output shaft radius.

$$\tau = Fr\tan(\theta) \tag{16}$$

$$\theta = \tan^{-1}\left(\frac{\tau}{Fr}\right) = \tan^{-1}\left(\frac{\tau_{\text{stall}}}{2Fr}\right) \tag{17}$$

Equation (17) only holds if we consider ideal angled roller behavior. We can express the effects of lateral slip and rolling resistance on the torque supplied from the motor using

$$\tau = \tau_{\text{motor}} - \tau_{\text{rr}} - \tau_{\text{slip}}. \tag{18}$$

We then substitute the contribution of the roller angle and output force into (18) to obtain another equation for the roller angle that includes the effects of lateral creep and rolling resistance.

$$\frac{1}{2}\tau_{\text{stall}} = Fr\tan(\theta - \alpha) + rC_{\text{rr}}F_n n_{\text{rollers}} + Fr\left(\tan(\theta) - \tan(\theta - \alpha)\right) \tag{19}$$

$$\theta = \tan^{-1}\left(\frac{\tau_{\text{stall}}}{2Fr} - \frac{rC_{\text{rr}}F_n n_{\text{rollers}}}{F}\right). \tag{20}$$

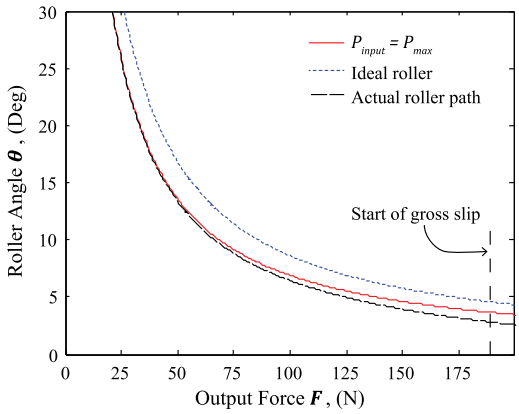

Fig. 4. Ideal roller angle shows an inverse relationship between roller angle and output force. The blue (dotted) line shows the relationship without losses to rolling resistance. The red (solid) line shows the relationship when rolling resistance is considered. The black (dashed) line shows the actual roller behavior when lateral slip and rolling resistance are considered. Gross slip occurs at $0.7\ F_n n_{\text{rollers}} \mu$.

By analyzing (20), it will quickly become apparent that the angle is not dependent on the lateral slip coefficient C_{slip}. This is because the amount of lateral slip only affects the power transferred from the roller to the shaft and not the total torque demanded of the motor. The rolling resistance, however, does affect the torque demanded by the motor. The desired roller angle as a function of output force is not the same as the path taken by the roller. The actual path and, therefore, the actual transmission ratio are calculated using (10), which includes the slip angles that are dependent on output force F.

B. Example Using 6-W DC Motor

Using an off the shelf brushless out-runner motor rated at 6-W peak power with stall torque τ_{stall} and free speed ω_{fs}, we can show an example of the roller angle profile described in (20). Fig. 4 shows a plot of the roller angle profile for the ideal case without losses, and for the case with rolling resistance. Also included in the plot is the roller path angle, which includes the effects of lateral slip. Table I shows the parameters used in the calculation of the roller angle. The values for the coefficient of rolling resistance C_{rr} and the coefficient of lateral slip C_{slip} were calculated empirically, with experimental values described in Section VI-B.

C. Effect of Roller Normal Force and Shaft Diameter

We can analyze the equations that govern the performance of the angled roller transmission to understand tradeoffs between the system parameters. One example is the effect of roller normal force, F_n. Fig. 5 shows the efficiency ε of the angled roller system, as described in (13), using parameters described in Table I, for three different values of normal force per roller, F_n. The possible output force increases linearly with an increase in roller normal force, but as illustrated in (11), the power loss to rolling resistance, P_{rr}, also increases. The power lost to lateral slip is also affected by the roller normal force. As shown in (12),

TABLE I
SYSTEM PARAMETERS USED IN DC MOTOR EXAMPLE

Parameter	Value	Units
P_{max}	5.97	Watts
τ_{stall}	48	N·mm
ω_{fs}	4850	r/min
r	1.5875	mm
μ	0.2	-
C_{rr}	0.00225	-
C_{slip}	6.086	degrees
n_{roller}	3	-
F_n	450	N per roller

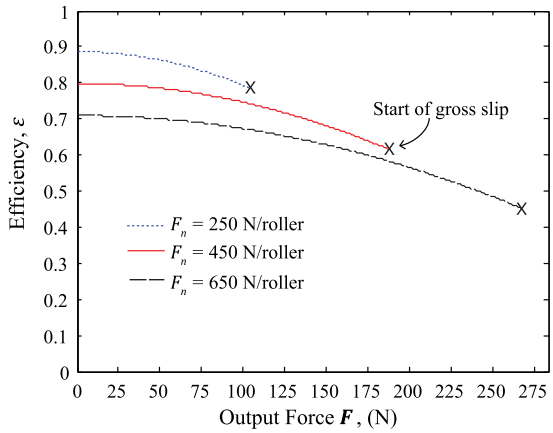

Fig. 5. Roller normal force affects the overall efficiency by altering the losses to rolling resistance and to lateral slip. With higher normal forces, higher overall output forces can be achieved at the cost of a lower overall efficiency. This plot is shown for a three-roller system.

for a given output force F, a higher amount of normal force will result in a reduction in the power lost to lateral slip P_{slip}. Since the key factor is the total normal force between the entire set of rollers and the shaft, the number of rollers used does not affect the performance or efficiency of the system. However, the more rollers used to distribute the normal force and output load, the lower the Hertzian contact stresses experienced at the roller-to-shaft interface.

Since rolling resistance acts as a force at the contact between the roller and the shaft, an increase in shaft diameter leads to increased losses to rolling resistance. As indicated in (12), the power lost to lateral slip also increases linearly with the shaft radius. Fig. 6 shows the efficiency ε of the angled roller drive system using the parameters from Table I with three different shaft radii. Although the efficiency effects show that a small drive shaft is preferable, the Hertzian contact stresses increase with a reduction in shaft radius.

IV. LINKAGE BEHAVIOR

The linkage system that houses the rollers in the rotating "nut" is based on the Watt straight-line mechanism originally developed for drafting purposes and then implemented in steam engines and automotive suspensions [20]. The Watt linkage provides a single DOF allowing near perfect linear translation at the

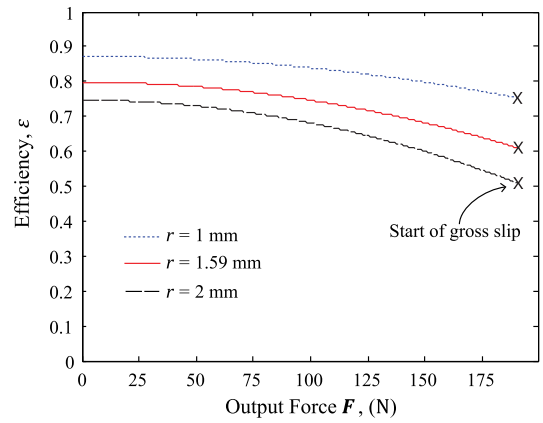

Fig. 6. Larger shaft radius dissipates more energy to rolling resistance. There is also an increase in energy lost to lateral slip since the same slip angle now is a greater portion of the total roller angle.

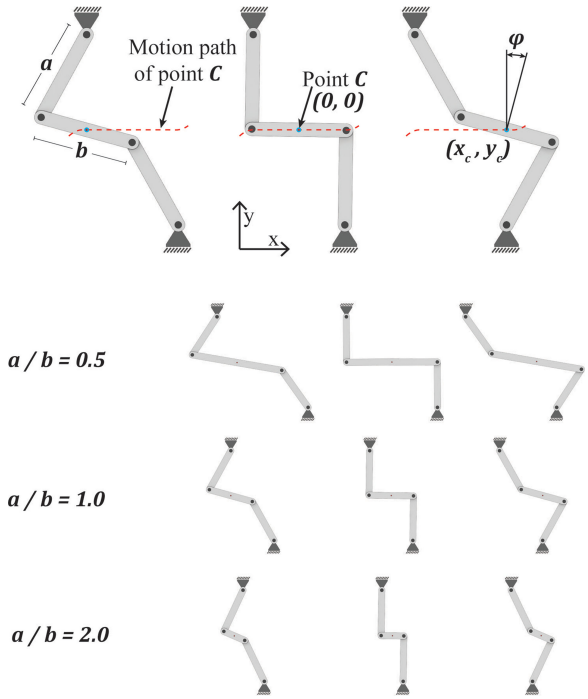

Fig. 7. Watt straight-line mechanism ensures point C travels along a straight-line path as indicated by the red (dotted) line. The position of C is described by (x_c, y_c) and is defined as being at $(0, 0)$, in the neutral configuration. The angle of the center bar with reference to vertical is φ. The ratio of length $\boldsymbol{a}$ to length $\boldsymbol{b}$ changes the relationship of angle change to lateral displacement of C.

midpoint of the center link, with an associated change in angle. The linear translation is required to maintain good contact on the shaft as the rollers translate relative to the rotating "nut." As compared with other straight-line mechanisms including the ChebyShev and Peaucellier–Lipkin [28], the angle change of the center bar is identical in both directions of movement, which ensures that the associated angle change from the neutral position is the same for pushing and pulling motions.

Fig. 7 shows the straight-line behavior of the mechanism and how the ratio of link lengths a and b affect the behavior. Since we are interested in using this system to alter the angle of a drive roller, we have studied the association between the movement of point C and the associated angle of the center link φ. Fig. 8 shows the effect of the link length ratios on the system behavior. The top plot shows vertical position of C as the mechanism deflects along the length of the output shaft, while the bottom plot shows the angle of the center link along the motion path. All length values are normalized by the length of a in order to examine the results nondimensionally. In Fig. 8, the angle of the center link was calculated using an inverse kinematics solver, but can be approximated for the straight-line region by (21) derived using the law of cosines and the linkage dimensions.

$$\varphi \approx \tan^{-1}\left(\frac{a}{b/2 + x_c}\right) - \cos^{-1}\left(\frac{b^2/2 + bx_c + x_c^2}{b\sqrt{a^2 + (b/2 + x_c)^2}}\right) \tag{21}$$

Since the drive roller of the proposed transmission is mounted in the center link at point C, a larger change in the angle of the center link will result in a larger change in roller pitch angle. This is constrained by the limits of straight-line motion of the mechanism. Table II shows the angle change of the center link at the point when point C begins to deviate from travel along a straight line. The suggested limits of 1% and 0.5% of length a were based on the packaging of the prototype detailed in Section VI. The singular boundary is the absolute limit created when links a and b are parallel. We can see based on this analysis of the effect of the a/b ratio that the optimal system will greatly depend on packaging since the a/b ratio should be maximized to increase the amount of possible angle change for a given tolerance to deviations from perfect straight-line behavior.

V. Compliance Tuning for Constant Power Application

In this section, we will combine the behavior of an angled roller transmission element (see Section II) and the linkage behavior (see Section IV) to yield a passively variable CVT that maximizes the mechanical power delivered from the drive motor. This is done by selectively tuning the compliance of the linkage system from the neutral position to match the desired force versus roller angle profile described in Section III-A.

Equation (20) shows the relationship between roller angle and shaft output force that results in the drive motor operating at maximum mechanical input power. Using (14), we can show the sensitivity of the mechanical input power to the roller angle as illustrated in Fig. 9. We will, therefore, try to optimize the stiffness of the four-bar-linkage system to match the optimal roller angle for all possible output loads.

In an attempt to match the desired optimal roller angle profile, we begin by choosing the initial roller angle θ_{initial} for the neutral position of the four-bar mechanism, as seen in Fig. 2(b). The resulting roller angle θ under deflection of the four-bar-linkage is described in (22), where φ is the angle of the center link.

$$\theta = \theta_{\text{initial}} - \varphi \tag{22}$$

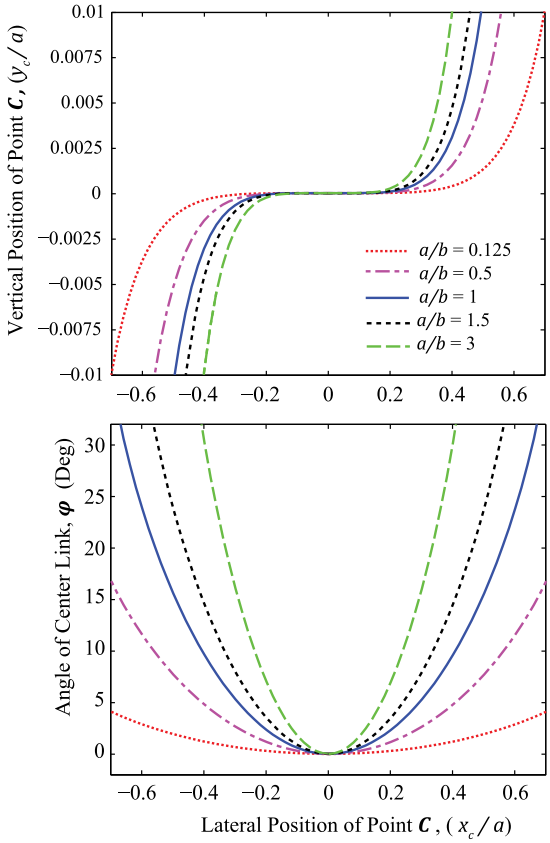

Fig. 8. These plots show the vertical displacement Y_C and angle of point C as a function of lateral displacement X_C. The values are normalized by the length of the vertical link a.

TABLE II
MAX ANGLE CHANGE FOR VARYING TOLERANCE TO STRAIGHT-LINE BEHAVIOR

	$y_c/a = 0.005$		$y_c/a = 0.01$		Singular Boundary*	
a/b	x_c/a	φ	x_c/a	φ	y_c/a	φ
0.125	0.628	3.18	0.700	4.10	0.161	9.66
0.25	0.560	4.92	0.620	6.00	0.160	16.26
0.50	0.496	7.57	0.560	9.89	0.138	25.53
1.00	0.438	11.65	0.495	15.24	0.100	36.87
1.50	0.405	14.91	0.459	19.61	0.076	43.87
2.00	0.383	17.79	0.434	23.44	0.060	48.75
3.00	0.354	22.80	0.401	30.33	0.041	55.25

*The singular boundary is defined as the position where link a and b become parallel.

For a chosen linkage length ratio a/b, we want to maximize the total angle change of the roller. We can solve for θ_{initial} by setting it equal to the max angle change of the center link φ for the desired *a/b* ratio linkage, as shown in Table II, and adding the desired angle of the roller at $0.7\, F_n n_{\text{rollers}}\, \mu$, since beyond this angle major losses occur to gross slip. This gives the maximum total angle change of the roller, for the desired a/b ratio linkage, over the possible output loads. Equation (21) gives the relationship between the center link angle, φ, and the lateral displacement x_c. We can, therefore, combine (21) and (20) to

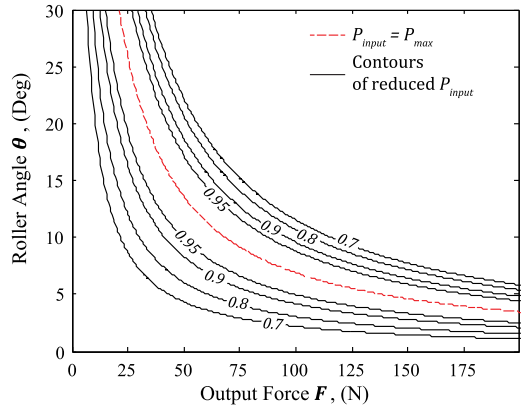

Fig. 9. Ideal roller angle as a function of output force is shown in the red line. Contours of reduced power input values show the input power sensitivity to maintaining the ideal roller angle profile.

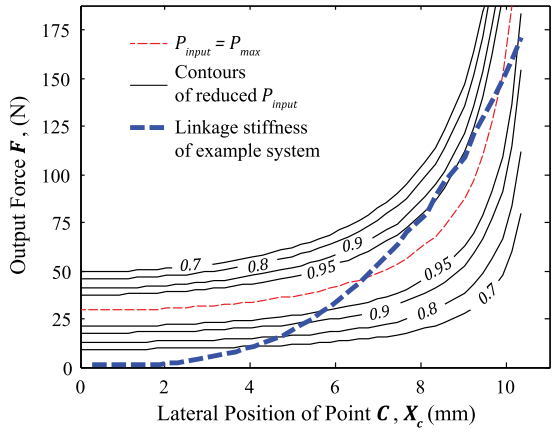

Fig. 10. Stiffness of the linkage when constrained using linear springs can be compared with the ideal stiffness profile to optimize peak input power. A fixed ratio transmission would operate on a vertical line positioned according to the chosen fixed ratio.

yield the desired compliance of the linkage system to maximize input motor power. The contours of Fig. 9 have been translated into a desired compliance of the linkage mechanism using the linkage kinematics, shown in Fig. 10, as approximated by (21) for a linkage with $a/b = 1.5$, $a = 22.5$ mm, and $b = 15$ mm.

Along with the ideal stiffness profile to maximize motor power input, Fig. 10 shows the stiffness profile achieved when the linkage system is constrained using linear springs as indicated in Fig. 11. Although this constraint strategy is unable to perfectly match the desired profile, we can see that the mechanical input power is greatly increased as compared with a fixed ratio transmission. Since each lateral position of point C represents a particular roller angle, a fixed ratio transmission would follow a straight vertical path through Fig. 10, thus only creating the desired motor operating conditions for a small range of output forces. For the simple case of constraining the linkage with linear springs, the motor is able to operate within 95% of the peak power input for output loads between 25 and 165 N. Limitations on the initial roller angle and the requirement for

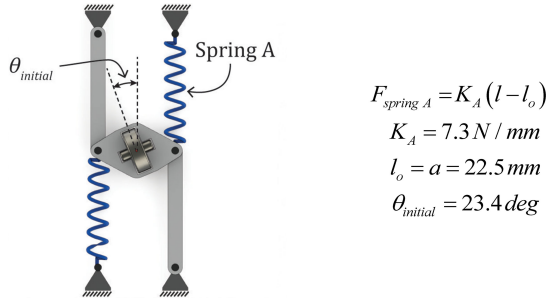

Fig. 11. Chosen linkage with $a/b = 1.5$, is constrained using two linear springs. The parameters of the springs were optimized to best match the desired stiffness profile. $F_{\text{spring}A} = K_A\ (l - l_o)\ K_A = 7.3\,\text{N/mm}\ l_o = a = 22.5\,\text{mm}\ \theta_{\text{initial}} = 23.4°$.

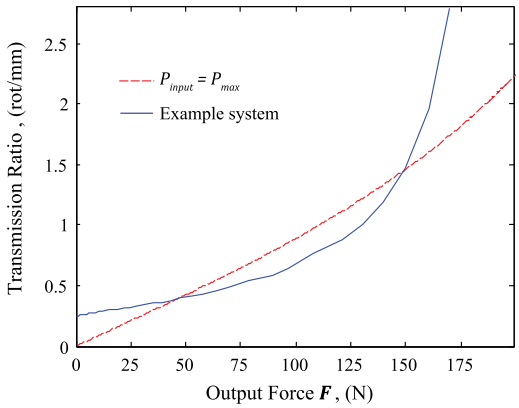

Fig. 12. Example of passive transmission system, which is designed to achieve maximum input power with parameters from Table I, achieves a range of transmission ratios from 0.23 to 2.8 rot/mm.

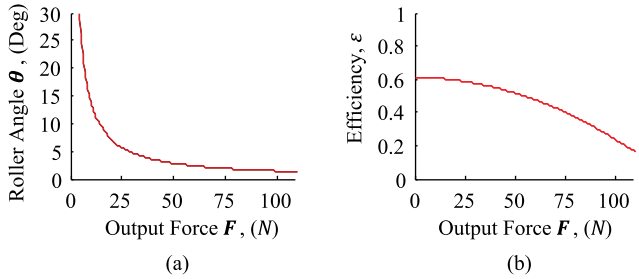

Fig. 13. (a) Desired roller angle profile to operate the integrated motor at peak electrical efficiency. (b) Predicted mechanical efficiency of the prototype transmission for the desired operating conditions.

static equilibrium at the neutral configuration prevent the system from tracking the ideal stiffness profile for small output forces.

The stiffness values shown in Fig. 11 represent the parameters necessary for a three roller system to achieve the overall desired stiffness. If the number of rollers is changed, the spring constants for the linear springs would also need to be altered to give the same overall system stiffness. Although there are numerous methods to alter the stiffness of the linkage system by adding spring elements to better match the desired stiffness profile, we have shown a single simple method that illustrates the proposed CVT concept. Fig. 12 shows that the rotary-to-linear transmission ratio, as described by (10), varies from 0.23 to 2.8 rot/mm over the entire range of output forces when rolling resistance and lateral slip are taken into account.

VI. Proof-of-Concept Design and Testing

A prototype passive variable transmission was developed as a proof of concept and a way to test the methods described above. Here, instead of maximum delivered mechanical power from the motor, we have tuned the transmission to operate at the peak electrical efficiency point of the actuator. Although this represents a different operating region of the motor (generally at one seventh of the stall torque of the motor over the entire operating range [22]), the design process is similar to what was laid out in Section V. We started by using (20) to determine the ideal roller angle profile using the new desired motor torque parameter. The desired profile is shown in Fig. 13(a). We were then able to compute the predicted mechanical efficiency of the system as a result of rolling resistance and lateral slip losses, as shown in Fig. 13(b).

As illustrated in Fig. 14(a), the prototype passive transmission system consists of two four-bar-mechanisms integrated into opposite sides of an aluminum rotating housing. The housing is 27.5 mm in diameter and holds the linkages, support bearings, and contains the magnetic rotor of an outrunner brushless DC motor (Turnigy 2830 Brushless Motor, 800 kV). An exploded view of the prototype is shown in Fig. 14(b). Within the center links of the four-bar linkages, the drive rollers are supported with two roller bearings. The rollers and output shaft are made from O1 oil-hardening tool steel, hardened to a Rockwell C58-62 surface hardness. Because of the large normal force required between the rollers and the shaft, the two center links are forced together using two bolts that can be adjusted to alter the roller normal force. Since these normal force bolts, as seen in Fig. 14(b), only squeeze the center links together, they have no effect on the motion of the linkages in response to a lateral output force from the rollers on the shaft. The a/b ratio for the linkages used in the prototype was 0.5 due to limitations related to the overall system diameter and the size of the drive roller support bearings. The initial roller angle was 7.0° within the center link. Fig. 14(a) shows the rubber springs used to constrain the motion of the four-bar linkages with respect to the rotating housing. These springs are initially positioned tangent to the movement of the linkages. The parameters of the springs were chosen to match the desire stiffness profile for the chosen linkage ratio. Similarly to Section V, this was computed using (20) and (21). Details on the system parameters used in the prototype including details on the integrated brushless motor are shown in Table III. Since only two rollers are used in the prototype and there is an upper bound to the allowable contact stress, the expected maximum output force of the prototype system is about 90 N before gross slip occurs. The overall weight of the prototype, as seen in Fig. 14(a), is 122 g.

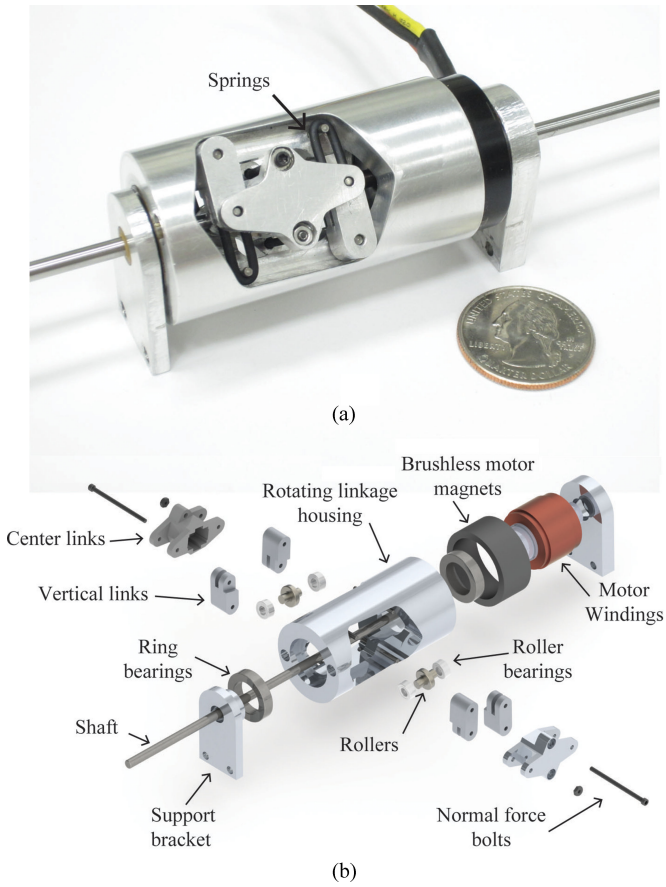

Fig. 14. Passively adaptive rotary-to-linear CVT. (a) Physical prototype with a US quarter for size reference. (b) Exploded view shows the component of the linkages, housing, and integrated brushless motor that rotates the entire housing around the shaft.

TABLE III
SYSTEM PARAMETERS OF PROTOTYPE PASSIVE TRANSMISSION

Parameter	Value	Units
P_{max}	4.6	Watts
τ_{stall}	48	N·mm
ω_{fs}	3800	r/min
V_{motor}	7.0	Volts
r	1.5875	mm
$r_{rollers}$	3.43	mm
$\theta_{initial}$	7.0	degrees
F_n	≈350	N per roller
$\sigma_{HertzMax}$	2.66	GPa
C_{rr}	0.00225	-
C_{slip}	6.086	degrees
n_{roller}	2	-

A. Experimental Test Setup

A custom testing apparatus was constructed to monitor the behavior of the proposed transmission system and drive motor under various output loading conditions. The testing apparatus shown in Fig. 15 consists of a brushless motor supported by a torsional load cell to measure the motor output torque. In the prototype system shown in Fig. 14(a), the entire housing and

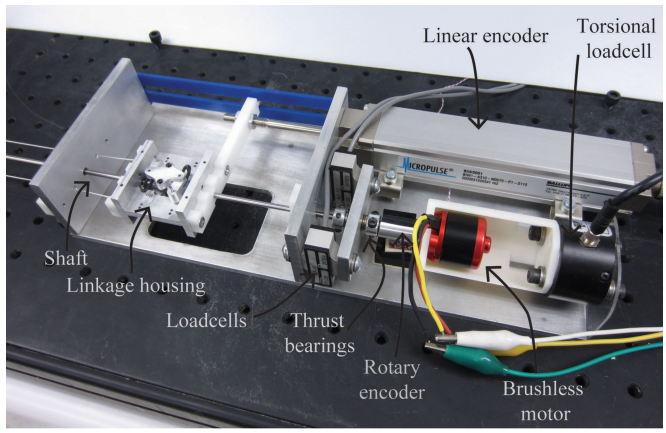

Fig. 15. Testing apparatus to evaluate performance of the passive transmission system.

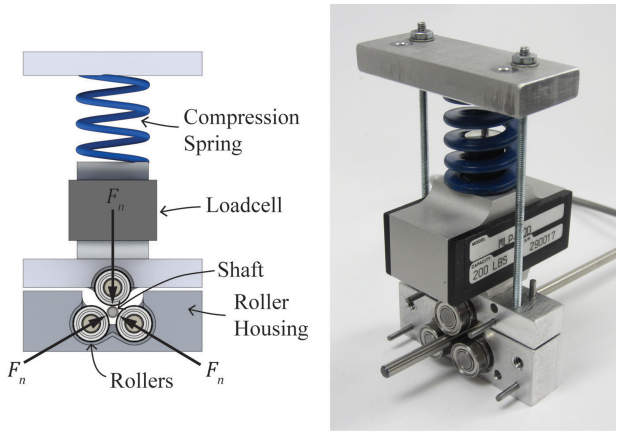

Fig. 16. Custom carriage was created that housed three rollers perpendicular to the shaft with direct measurement of the normal force. (a) Schematic of three roller system with load cell and (b) view of testing system with front half removed to show rollers and bearings.

linkages rotate around a center shaft and produce a lateral force on the shaft. In the testing apparatus, however, the shaft is rotated to produce a lateral force on the linkage housing. Although this does not change the behavior of the transmission, it makes it easier to monitor the movement of the four-bar-linkage system under load. The rotation of the shaft and linear movement of the linkage housing are directly measured with encoders. The lateral force between the rollers and the shaft is also measured directly by measuring the reaction loads between the shaft and frame using load cells.

In addition to testing the behavior of the proposed transmission as a system, we also constructed a testing setup to evaluate the parameters of rolling contact required to calculate an accurate roller angle profile. Fig. 16 illustrates the test setup used to evaluate the coefficients of rolling resistance and lateral slip. A custom carriage was developed that held three rollers at a fixed angle perpendicular to the output shaft. The normal force was

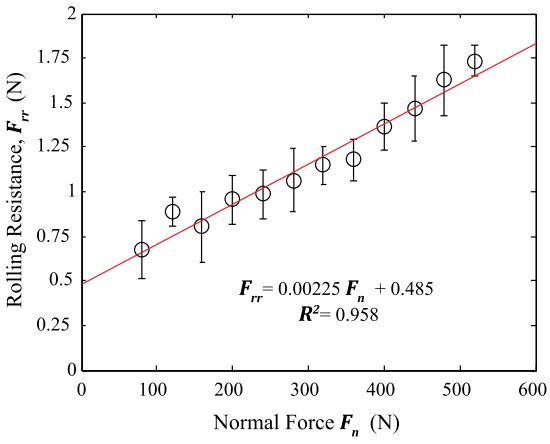

Fig. 17. Rolling resistance force is shown to exhibit a linear increase with respect to the normal force applied between the roller and the shaft. In this example, the rollers were made from O1 tool steel, hardened to rockwell-58-62 surface hardness with maximum Hertzian contact stress of 2.41 GPa.

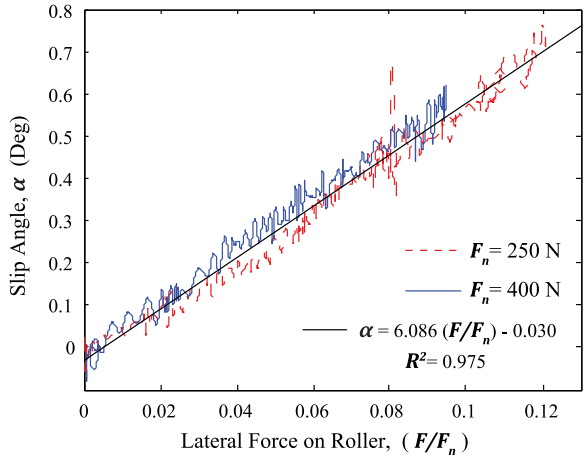

Fig. 18. Lateral slip coefficient measurement using the roller testing carriage. The linear relationship holds for up to 70% of μ before gross slip occurs.

directly altered and measured using a load cell, as illustrated in Fig. 16(a).

B. Experimental Testing Results

1) Rolling Resistance: In order to measure the coefficient of rolling resistance as described in (6), the three-roller carriage shown in Fig. 16 was assembled into the system testing apparatus in place of the moving linkage housing. The compression spring was then compressed to place an equal normal force between all three rollers and the shaft. By powering the brushless motor and measuring the resultant torque, we were able to determine the linear relationship between normal force in the rollers and the force of rolling resistance. Fig. 17 shows the measured rolling resistance force $F_{\rm rr}$ for 12 values of roller normal force ranging between 80 and 520 N. Here, the error bars represent $\pm$ one standard deviation of all rolling resistance values measured at 2000 Hz over a 5-s trial at 4500 $\pm$ 600 rot/min. It is important to remember that the measured value of rolling resistance is the combination of losses occurring at the roller to the shaft contact patch as well as the losses within the bearings that support the rollers. The non-zero rolling resistance force at zero roller normal force is a result of other losses within the testing apparatus not related to the normal force of the rollers. The rollers and shaft were made from O1 oil-hardened tool steel, hardened to a Rockwell C58-62 surface hardness. The Hertzian contact stress at the roller to shaft interface calculated for the largest value of normal force was 2.41 GPa. Using a linear fit to the measured data, we show a rolling resistance coefficient $C_{\rm rr} = 0.00225$.

2) Lateral Slip: Using the same roller carriage, the lateral slip coefficient could be directly measured. With a set normal force on the three rollers, load was placed on the entire carriage along the direction of the output shaft. Since the system testing apparatus allows us to measure the lateral load, carriage position, and the shaft speed simultaneously, we can calculate the relative slip angle occurring at the roller/shaft interface using (23). Here, $V_{\rm carriage}$ represents the lateral velocity of the roller housing within the testing apparatus

$$\alpha = \tan^{-1}\left(\frac{V_{\rm carriage}}{r\omega}\right). \tag{23}$$

Fig. 18 shows the measured slip angle for two values of normal force per roller. Since the lateral force on the rollers is normalized by the roller normal force, the resulting coefficient is in the units of degrees. A linear fit to both trials results in a lateral slip coefficient of $C_{\rm slip} = 6.086°$. As shown by Gillespie *et al.* [23], the linear trend is valid for up to 70% of μ.

3) Transmission Behavior: We showed in Fig. 12 that achieving the correct linkage stiffness profile was a key to achieving the correct transmission ratio over the range of output forces. Using the testing apparatus, we were able to compare the desired and actual stiffness profile achieved by the prototype linkage system. Fig. 19 shows the ideal stiffness for the a/b ratio of the prototype to give maximum electrical efficiency of the drive motor. Also shown is the measured stiffness of the prototype system. The hysteresis in the measure stiffness curves is a result of the rubber spring elements used in the prototype.

With the same linkage and constraining springs used in the prototype, now placed in the linkage housing of the testing apparatus, the overall performance of the passive transmission system was evaluated. The brushless motor (identical to the motor integrated into the prototype transmission), was supplied 7.0 V to rotate the shaft. As the linkage housing moved laterally, it pulled against a linear spring. As the load on the system increased, the linkages began to deflect and alter the transmission ratio of the system. Because we directly measured the load, output velocity, input torque, and input motor speed, we are able to characterize the transmission.

Our overall goal in the tuning of this particular prototype transmission was to allow the motor to operate at the point of peak electrical efficiency. Fig. 20 shows the motor performance curves as well as the desired operating point. The motor torque curves were measured on the same testing apparatus by applying an external torque to the output shaft. We would expect that for a fixed transmission ratio, a variable load would result in the

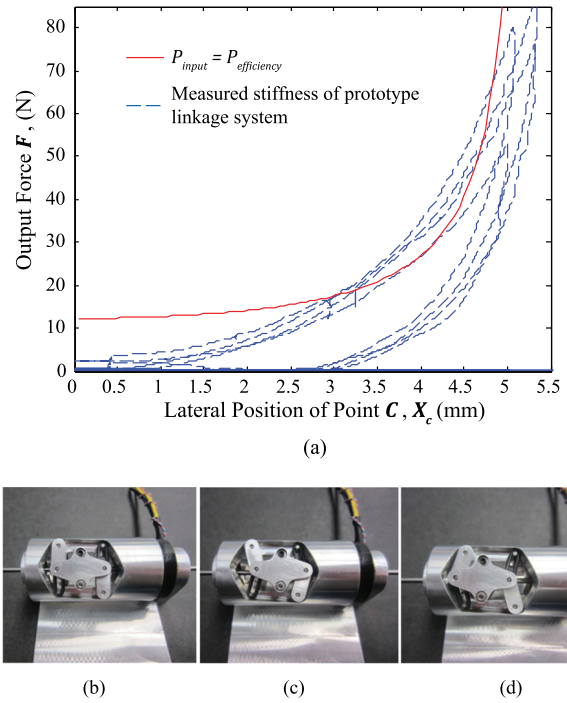

Fig. 19. Measured stiffness of the prototype transmission linkage system. The red (solid) line shows the desired profile. The blue (dashed) line shows the measured stiffness of the prototype system over repeated cycles of loading. (b) Neutral configuration under zero output load, (c) deflected position under a 75-N pulling load, and (d) deflected position under a 75-N pushing load.

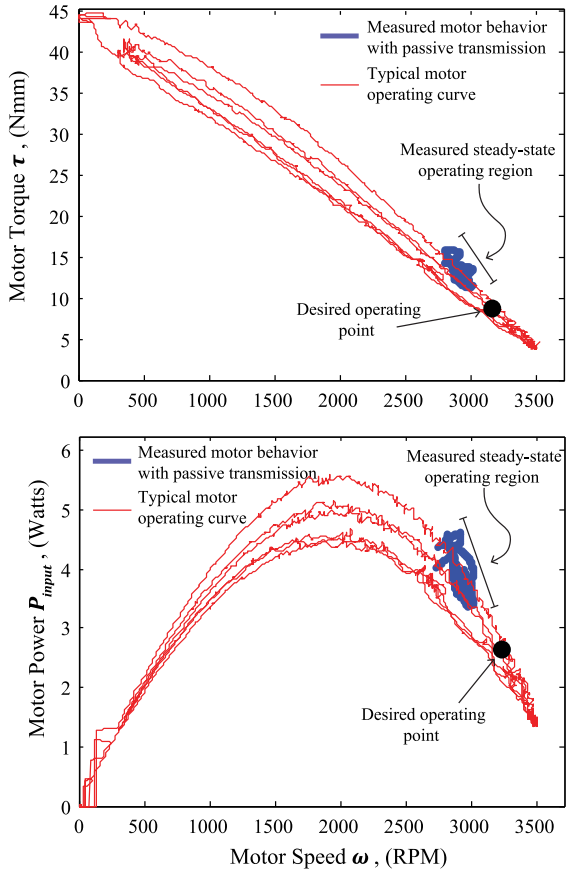

Fig. 20. Operating range of the motor was measured while an output force was swept from 0 to 75 N. The red curves represent the measured typical motor behavior for repeated cycles of loading and unloading. The operating range of the motor while using the passive transmission is compared with the typical motor behavior, as well as with the desired operating point for peak electrical efficiency.

motor sweeping across the entire operating range. This is due to the fact that the motor needs to increase the applied torque to compensate for the increased output load. Using the passive roller transmission, however, the motor torque would be constant over the range of loads at the output. In Fig. 20, we show the resulting steady-state operating behavior (blue curve) of the motor during a trial in which the output load, F, is varied from 0 to 75 N, while using the passively variable transmission. Although the motor does not operate exactly at the desired operating point, the transmission is correctly altering the transmission ratio in order to keep the demanded torque of the motor in a 5-N $\cdot$ mm range.

Over the entire range of output loads between 0 and 75 N, the mechanical efficiency of the system ranged between 30 and 18%. The efficiency was measured by determining the ratio of the output mechanical power, $V * F$, to the mechanical input power from the motor, $\tau * \omega$. The measured efficiency values were lower than calculated in Fig. 13(b), likely due to a larger than expected coefficient of rolling resistance.

Since gross slip occurred at about 80 N, the efficiency quickly drops off after a maximum 75 N output force. The measured transmission ratio within that range varied between 1.12 and 4.79 rot/mm.

VII. Applications in Robotics

The proposed transmission system has the potential to improve efficiency and power-to-weight ratio over existing single-ratio rotary to linear transmission systems. The most likely comparison is the use of this transmission over a single pitch lead screw in a robotic system such as a leg or robotic hand. If the loading of the system is very well characterized, then the pitch of the lead screw and motor can be properly chosen to maximize efficiency or power from the motor. However, if the loading is highly variable, then this actuation method will be highly inefficient over a portion of the loading. For highly variable loading conditions, as are experienced in most robotic systems such as robot arms, hands, or legs, this transmission can help to optimize power output. As stated in earlier sections, the efficiency and weight savings gained from operating at the most efficient or most powerful operating point of the motor must be weighed against the reduced efficiency of friction drive-based systems. These tradeoffs depend on the scale of the transmission system and the priorities of the robot design.

Although lead screw designs are commonly used for precise positioning, they are less desirable for force-based control systems due to their limited backdrivability. The proposed transmission incorporates a series-elastic element that makes the system better suited for force/torque control instead of position control. Position control of series elastic systems can still be achieved with proper closed-loop control methods.

VIII. Conclusion and Future Work

In this paper, we have presented a novel concept for a variable transmission that can be designed to passively vary with the output load conditions in order to keep the actuator acting near a desired/optimal point. Besides this key feature, the concept has a number of additional benefits, including simple and compact packaging, one of the few rotary-to-linear CVTs that have been developed, and has a built-in overload protection that can be tuned by adjusting the normal force on the rollers. After laying out the key parameters affecting the design and performance of these systems and showing how to design for two example applications, we presented the design and evaluation of a proof-of-concept device. Our results showed good performance for a first prototype in a controlled test.

There are a number of aspects of the described concept that we would like to investigate in the future. One direct extension involves moving past the steady-state behavior analysis to look at behavior during accelerations, which is important not only for start-up phases but for transients during applications such as position tracking as well. Another aspect to this type of transmission that we would like to examine is its series elastic behavior and general impedance properties. In particular, due to the Watt linkage, linear translation of the output is tied to the pitch angle of the rollers, and it is not clear how driving this motion from the output will affect the reflected stiffness. As with any actuator with nontrivial compliance at the output, there will be issues related to control that should also be investigated in future work [29].

One of the key areas for future improvement of the concept relates to improving the efficiency of future prototypes, without which many of the benefits of variable transmission will not be able to be realized. The measured efficiency of the prototype actuator was less than predicted using the measured values of rolling resistance and lateral creep. In the three-roller testing carriage to test for rolling resistance, larger bearings were used to support the driver rollers. In the prototype system, miniature roller bearings were required for packaging reasons. The added rolling resistance of the smaller roller bearings is likely the cause for both the decreased efficiency of the system, as well as the slight shift in measured motor torque from the desired value in Fig. 20. Since the effect of rolling resistance acts as a fixed torque for a given setup, designing the system for a higher torque operating point, or choosing a motor with higher torque output, would result in a higher mechanical efficiency of the transmission. More developed products with the roller transmission element have a reported efficiency of 75%, and we expect that fully engineered and professionally made future versions of our system will have comparable efficiencies [16].

Acknowledgment

The authors would like to thank L. Odhner, S. Hall, and S. Backus for their helpful discussions regarding the topics presented in this paper.

References

[1] D. A. Winter, *The Biomechanics and Motor Control of Human Gait: Normal, Elderly and Pathological*, 2nd ed. Waterloo, ON, Canada: Univ. Waterloo Press, 1991.

[2] G. R. Schulz, "End effector with load-sensitive digit actuation mechanism," U.S. Patent US5 280 981 A, Jan. 1994.

[3] P. Setlur, J. R. Wagner, D. M. Dawson, and B. Samuels, "Nonlinear control of a continuously variable transmission (CVT)," *IEEE Trans. Control Syst. Technol.*, vol. 11, no. 1, pp. 101–108, Jan. 2003.

[4] J. Kim, H. Yeom, F. C. Park, Y. I. Park, and M. Kim, "On the energy efficiency of CVT-based mobile robots," in *Proc. IEEE Conf. Robot. Autom.*, 2000, pp. 1539–1544.

[5] H. Yamada, "A radial crank-type continuously variable transmission driven by two ball screws," in *Proc. IEEE Conf. Robot. Autom.*, 2012, pp. 1982–1987.

[6] M. Okada and Y. Takeda, "Optimal design of nonlinear profile of gear ratio using non-circular gear for jumping robot," in *Proc. IEEE Int. Conf. Robot. Autom.*, May 2012, pp. 1958–1963.

[7] E. L. Faulring, J. E. Colgate, and M. A. Peshkin, "The cobotic hand controller: Design, control and performance of a novel haptic display," *Int. J. Robot. Res.*, vol. 25, no. 11, pp. 1099–1119, Nov. 2006.

[8] (2006, Nov.). LandRider, Baltimore, MD, USA. [Online]. Available: www.landriderbikes.com/features.html

[9] O. S. Cretu and R. P. Glovea, "Constant power continuously variable transmission (CP-CVT): Operating principle and analysis," *J. Mech. Des.*, vol. 127, pp. 114–119, Jan. 2005.

[10] J. Lemmens, "Continuously variable automatic transmission," U.S. Patent 3 850 050, Nov. 1974.

[11] T. Takaki and T. Omata, "Load-sensitive continuously variable transmission for robot hands," in *Proc. IEEE Int. Conf. Robot. Autom.*, New Orleans, LA, USA, Apr. 2004, 3391–3396.

[12] T. Hagiwara and S. Hirose, "Development of dual mode X-screw: A novel load-sensitive linear actuator with a wide transmission range," in *Proc. IEEE Conf. Robot. Autom.*, 1999, pp. 537–542.

[13] K. Matsushata, S. Shakanai, and H. Yokoi, "Development of drum CVT for a wire-driven robot hand," in *Proc. IEEE/RSJ Int. Conf. Intell. Robots Syst.*, St. Louis, MO, USA, 2009, pp. 2251–2256.

[14] J. Ingvast, J. Wikandaer, and C. Riderstorm, "The PVT, an elastic conservative transmission," *Int. J. Robot. Res.*, vol. 25, pp. 1013–1032, 2006.

[15] S. Hirose, H. Ohno, T. Mitsui, and K. Suyama, "Design of in-pipe inspection vehicles for d25, d50, d150 pipes," presented at the IEEE Int. Conf. Robot. Autom., Detroit, MI, USA, 1999.

[16] (2012). Model RG linear drives for reciprocating motion applications. [Online]. Available: http://www.amacoil.com/rg-linear-drives.html

[17] (2012). Linear motion control.[Online]. Available: http://www.zero-max.com/linear-motion-control-c-24-l-en.html

[18] G. A. Pratt and M. M. Williamson, "Series elastic actuators," in *Proc. IEEE Int. Conf. Intell. Robots Syst. Human Robot Interact. Cooperative Robots*, Aug. 5–9, 1995, vol. 1, pp. 399–406.

[19] R. Van Ham, T. G. Sugar, B. Vanderborght, K. W. Hollander, and D. Lefeber, "Compliant actuator design," *IEEE Robot. Autom. Mag.*, vol. 16, no. 3, pp. 81–94, Sep. 2009.

[20] F. D. Jones, *Ingenious Mechanisms for Designers and Inventors*. New York, NY, USA: Industrial, 1967.

[21] E. L. Faulring, J. E. Colgate, and M. A. Peshkin, "Power efficiency of the rotational-to-linear infinitely variable cobotic transmission," *J. Mech. Des.*, vol. 129, pp. 1285–1293, Dec. 2007.

[22] M. E. Brokowski, S. Kim, J. E. Colgate, R. B. Gillespie, and M. Peshkin, "Toward improved CVTs: Theoretical and experimental results," in *Proc. ASME Int. Mech. Eng. Congr. Expo.*, Nov. 2002, pp. 855–865.

[23] R. B. Gillespie, C. A. Moore, M. Peshkin, and J. E Colgate, "Kinematic creep in a continuously variable transmission: Traction drive mechanics for cobots," *J. Mech. Des.*, vol. 124, pp. 713–722, Dec. 2002.

[24] K. Johnson, *Contact Mechanics*. Cambridge, U.K.: Cambridge Univ. Press, p. 427, 1985.

[25] (2013, Aug.). Understanding DFTV Design. Ultimate Transmission. [Online]. Available: ultimatetransmissions.com/ut.php?DOWNLOADS

[26] D. Tabor, "The mechanism of rolling friction. II. The elastic range," *Proc. Royal Soc. London*, vol. 229, pp. 198–220, Apr. 1955.

[27] (2013, Jul.). Machine optimization through DC Motor selection. Maxon Motor Inc. [Online]. Available: www.maxonmotorusa.com

[28] A. B. Kempe, *How to Draw a StraightLine (A Lecture on Linkages)*. New York, NY, USA: Macmillan, 1877.
[29] S. P. Buerger, "Stable, high-force, low-impedance robotics actuators for human-interactive machines," Ph.D. dissertation, Dept. Mech. Eng., Mass. Inst. Technol., Cambridge, MA, USA, 2001.

Joseph T. Belter received the Bachelor's degree in mechanical engineering from the University of Michigan, Ann Arbor, MI, USA, in 2008 and the Master's degree from Yale University, New Haven, CT, USA, in 2011. He has been working toward the graduate degree with the Department of Mechanical Engineering and Material Science, Yale University, since September 2009.

His major research interests include robotic grasping and manipulation with applications in upper limb prosthetic devices.

Aaron M. Dollar (SM'13) received the B.S. degree in mechanical engineering from the University of Massachusetts, Amherst, MA, USA, and the S.M. and Ph.D. degrees in engineering sciences from Harvard University, Cambridge, MA, USA, and conducted two years of Postdoctoral research with the MIT Media Lab.

He has been an Assistant Professor with the Department of Mechanical Engineering and Materials Science, Yale University, New Haven, CT, USA, since January 2009. His research interests include human and robotic grasping and dexterous manipulation, mechanisms and machine design, and assistive and rehabilitation devices, including upper limb prosthetics and lower limb orthoses.

Dr. Dollar is a Cofounder and Editor of Robotics CourseWare.org: an open repository for robotics pedagogical materials. He received the 2013 DARPA Young Faculty Award, the 2011 Young Investigator Award from the Air Force Office of Scientific Research, the 2010 Technology Review TR35 Young Innovator Award, and the 2010 NSF CAREER Award.